



Computational Fluid Dynamic Analysis of Amphibious Unmanned Aerial Vehicle

Balasubramanian Esakki¹, P. Gokul Raj¹, Lung-Jieh Yang², Ekanshu Khurana³,
Sahadatan Khute³, P. Vikram¹

¹ Department of Mechanical Engineering, Vel Tech Rangarajan Dr Sagunthala R & D Institute of Science and Technology, Avadi, Chennai-600062, Tamilnadu, India

² Department of Mechanical and Electromechanical Engineering, Tamkang University, 25137, Tamsui, Taiwan, R.O.C.

³ Department of Aeronautical Engineering, Vel Tech Rangarajan Dr Sagunthala R & D Institute of Science and Technology, Avadi, Chennai-600062, Tamilnadu, India

Received January 15 20xx; Revised March 20 20xx; Accepted for publication June 20 20xx.

Corresponding author: B. Esakki (esak.bala@gmail.com)

© 2020 Published by Shahid Chamran University of Ahvaz

& International Research Center for Mathematics & Mechanics of Complex Systems (M&MoCS)

Abstract. Unmanned Aerial Vehicles (UAVs) are becoming popular due to its versatile maneuvering and high pay load carrying capabilities. Military, navy and coastal guard makes crucial use of the amphibious UAVs which includes the working functionalities of both hover craft and multi-rotor systems. Inculcation of these two systems and make it as amphibious UAV for water quality monitoring, sampling and analysis is essential to serve the human-kind for providing clean water. On this note, an amphibious UAV is designed for carrying a water sampler mechanism with an on-board sensor unit. In order to examine the stability of designed UAV under diverse wind load conditions and to examine the aerodynamic performance characteristics, computational fluid dynamic analysis (CFD) is performed. For various flight conditions such as pitch, roll, yaw and hovering, the flow characteristics around the vehicle body is examined. The aerodynamic phenomenon at the rotor section, vortex, turbulent regions, wake and tip vortex are identified. In addition, CFD analysis are conducted to determine the thrust forces during forward and hovering conditions through varying the wind speed 3 to 10 m/sec and speed of rotor 2000 to 5000 rpm. The effect of non-dimensional parameters such as advance ratio and induced inflow ratio on estimating the thrust characteristics are studied. Simulation results suggested that at 5° angle of attack and 8 m/sec wind speed condition, the aerodynamic performance of the vehicle is superior and stable flight is guaranteed. The amphibious UAV with flying and gliding modes for collecting water samples in remote water bodies and also in-situ water quality measurement can be well utilized for water quality monitoring.

Keywords: RANS Model, Amphibious vehicle, Multi rotor interaction, CFD.

1. Introduction

Unmanned Aerial Vehicles (UAVs) are becoming well sought after owing to its versatile maneuvering and payload characteristics for the deployment of various applications [1] including power line inspection, environmental monitoring, hyper spectral imaging and crop monitoring in Agricultural, telecom tower inspection, elevated infrastructure assessment, societal and disaster missions etc. However, the Amphibious UAV is a versatile tool for collecting water samples from various locations of inland remote water bodies and inaccessible regions [2]. The characteristics of unmanned and complexities of terrains in the alien region are demanding for the vehicle to operate in different modes like flying in the air as multirotor to reach the inspection site in short span of time and hovering on the water surface as hovercraft to collect water samples

Accurate prediction of amphibious UAVs aerodynamic phenomenon is a challenging task using Computational Fluid Dynamics (CFD). Despite of its scope, rotors interaction of amphibious UAVs have been considered by few researchers in examining the aerodynamic phenomenon, because of the following reasons. Firstly, rotor section's aerodynamic interaction is very challenging, as it brings out a complex multidisciplinary problem that involves wake flows, vortex, turbulence, rotor blade dynamics, and tip vortex [3][4]. Second, the interactional aerodynamics study is limited due to complex flow physics involving hover craft and multi rotor configuration along with the geometric complexity [5]. Concerning these reasons, major part of the published works is concerned with wind-tunnel experiments with idealized fuselage shapes mounted with generic helicopter rotors [6-7]. Rotary wing vehicles have proven to be of great advantage in multifaceted environments, while compared to fixed and flapping wings UAVs, owing to their superior hovering characteristics [8-9]. The aerodynamic behavior of rotors is the key factor in the functioning and controlling of such vehicles. The flow around the multirotor and interaction effect seems to be a complex issue in terms of achieving superior stability. Performing CFD analysis can reveal the various aerodynamic phenomenon such as vorticity, turbulence, wake area, tip vortex and other fluid structure interactions [10-12]. Celic et al. [13] (2006) compared experimental and CFD analyses of aerodynamic loads on rotor blades. In addition, they have identified that wake effect on rotor

field stream has critical effect in stabilizing the vehicle. It is inevitable to perform CFD examination to investigate the rotor wake zones and tip vortices. A novel UAV with an amphibious capability which can land on water as well as on ground and also flying on air is considered to break down the streamlined associations in this exploration [2]. Bewildering stream fields, vorticity and disturbance routines are caused by the unusual geometry of the vehicle and dealing with multiphysics is of great concern in addressing the fluid dynamics of UAV [14].

In this work, a novel amphibious vehicle to examine the aerodynamic interactions is accounted for. The designed vehicle is a result of thoroughly inculcating the features of hovercraft and multi rotor. A mechanism to collect water sample is configured at the middle region of the vehicle. Intricate flow fields are revealed due to the complex geometry of the vehicle causing vorticity and turbulence regimes which is crucial in examining the flow characteristics. Inspections using helicopter rotor interaction is an extraordinary subject of research [15]. In view of this, CFD studies are performed for various flight circumstances such as pitch up, journey, dynamic slow down and rapid tail shake. Antoniadis et al. [7] found that the flow interaction are higher and are dominated by separation over the downstream region of the fuselage backdoor and rotor hub which present the principal disagreements for all test cases. Investigation on experimental results are distinguished with CFD inspection of helicopter model equipped with unsteady sensor positions configured all over the fuselage at various cross-sectional planes. Weight on fuselage and rotors have been assessed and reviewed the liquid – structure conditions by Biava et al. [10]. Boyd et al. Ye, L. [14] investigated the hybrid model of coupling a rotor/fuselage flow field and a rotor loading model in way to present time accurate and time averaged rotor in flow ratios and the unsteady surface pressure on fuselage caused by blade passage. The difference in velocity between the two sides of rotors creates unbalance of the vehicle with respect to the maneuvering moment. Qijun et al. [16] brought out that the rotor flow field which is significantly affected by the effect of wake that resulted in affecting the performance of the vehicle. The wake effect leads to induced velocity and pressure regimes with an intense vorticity of flow influenced the lift characteristics. Cao et al. [17] emphasized that the CFD analysis carries great necessity in order to investigate the turbulence phenomenon, tip vortices and rotor wake regions. Simulation is carried out in the hovering mode for the wake effect of a rotor and semi-empirical correction for the vortex core effect. Conlisk et al. [18] performed experimental analysis of aero elasticity of blades and the blade vortex interactions is evaluated. Dindar et al. [19] carried out the melded flexible forced segment technique to consider the regions which are affected through vertical surges of rotor edges. A topology-based vortex focus revelation outline in uniting with an additional oversight measure is used to choose the vortex stream features of rotor bleeding edges. Domenge et al. [20] conducted numerical study to scan the blade-vortex interaction (BVI) appearance of rotorcraft using potential stream theory. Analysis using seeder assembly for various ascent angle and relating drag pressure to deduce the efficient execution of aerodynamic performance of UAV is carried out using CFD examination by Felismina et al. [21]. Filippone et al. [22] approximated the drag of rotorcraft fuselage for various courses of action and looking at point of conjunction of weight schedules are settled. Flow stream visualization inspection are coordinated for lopsided stream configuration and changed geometrical configuration using wind tunnel. Qijun et al. [23] anticipated the unsteady streamlined flow attributes of helicopter rotors using three-dimensional and transient discretization method. Characteristic mathematical plans like Roe-WENO, JST and Roe-MUSCL are executed to optimally choose convective movements. A viscous wake model (VWM) was generated by Shi et al. [24] to speculate the fundamental distortion of the helicopter blade and the rotor wake dynamics. Likewise, concordance quick weight scattering and span estimation of force of rotor blade is conducted. Aerodynamic interaction between tail rotor, fuselage and essential helicopter's rotor has been studied by Steijl et al. [6]. Through the assessment of rotor loading and weight co-powerful at transformed azimuth angle is settled. The prediction of unsteady aerodynamics rotor wake of helicopter is done by the method of full-span free wake method for forward flight and hover conditions and CFD inspection is validated with experimental results. Regardless, Tan and Wang [25] carried out very few inspections for unraveling the streamlined implementation traits of quad-copter. Lopez et al. [26] considered the stream around a quad-copter propeller using SA and K- ω models so that the velocity, wake districts and weight fields are settled for different rotating rates using moving reference frame (MRF) method. Thibault et al. [27] employed LES turbulence modeling layout and Lattice-Boltzmann, the vortex phenomenon of quad-copter. Yoon et al. [28] revealed that the vertical force of a quadrotor in hover phase is significantly affected with respect to the rotor separation distance under the study of multi-rotor flow interactional aerodynamics. It is evident from the review of literature that, CFD analysis of amphibious vehicle and flow interactions of multi-rotors under various motion characteristics is not examined. Exact solution of flow characteristics around the amphibious vehicle is imperative and is widely considered to be a daunting task to tackle. As far as our knowledge, there is no research that is being done in CFD simulation for aerodynamic performance of amphibian UAV and hovering conditions to observe the flow characteristics over the amphibian vehicle body. The objective of present work is to examine the interaction of rotors (flow characteristics) for various speeds, maneuvering (roll, pitch, yaw and hovering), wind conditions and reducing the drag for the novel amphibious UAV. CFD analysis of amphibious vehicle for pitch, roll, yaw and hovering conditions to observe the flow characteristics around the vehicle body are performed. In addition, amphibious vehicle without and with canopy to estimate the drag and the aerodynamic performance measures such as advance ratio and induced flow ratio are determined for varied rotor speeds. The aerodynamic phenomena at the rotor section are identified. Simulations are performed by changing the wind speed condition 3 to 10m/s and speed of rotor 2000 to 5000 rpm.

2. Computational Domain

The design of amphibious vehicle is conceptualized in CATIA V5 software platform and simulation analysis is performed using ANSYS Fluent V16.2. In order to reduce the buoyancy effect, the computational domain for conducting CFD analysis is made 10 times greater than the conceptual model as a rectangular enclosure as depicted in Fig. 1. The convective and diffusive coefficient with second order discretization of model is considered to perform incompressible fluid flow analysis. For the atmospheric pressure conditions with an air density of 1.2kg/m^3 , dynamic viscosity of $1.85 \times 10^{-5}\text{ kg/m.s}$ and a temperature of 30°C , simulations is carried out. The convergence criteria of 1×10^{-5} is accounted to obtain highly accurate solution. In addition, multirotor frame (MRF) model shown in Fig. 2 is created for simulating the propeller rotation through varying the speed.

3. Mesh Generation

The fluid-structure domain is created using ANSYS ICEM platform with a tetrahedral element mesh of 18,00,000 number of elements in the computational grid. The mesh quality is verified through skewness property that is close to zero as shown in Fig. 3(a) and orthogonality is about 0.9 for the most of the elements as shown in Fig. 3(b). In addition, grid independence test is performed to confirm the convergence of results with a greater accuracy.

Fig. 4 shows the structured meshed of the UAV model along with the boundary wall. The total number of elements and nodes after meshing are found to be 16, 86, 871 and 20, 43, 304 respectively. The assembly method adopted for solving is cut cell, smooth transition ratio of 0.272 is maintained. Corresponding minimum and maximum proximity size are found to be $5 \times 10^{-6}\text{ m}$ and $4.096 \times 10^{-2}\text{ m}$. Fig. 5 shows the zoom in view of the UAV inside the computational domain.

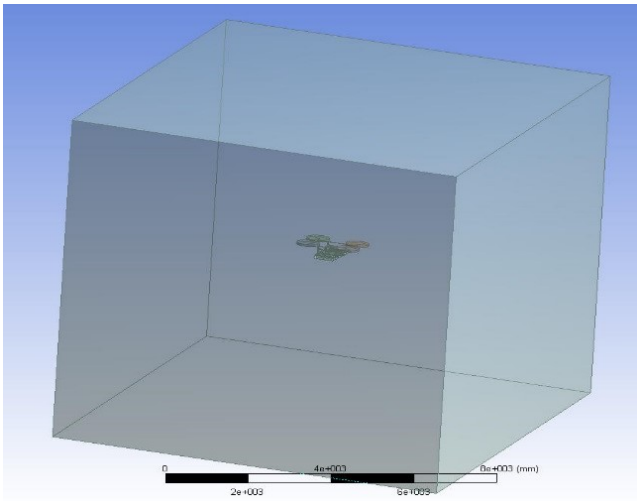


Fig. 1. Computational domain

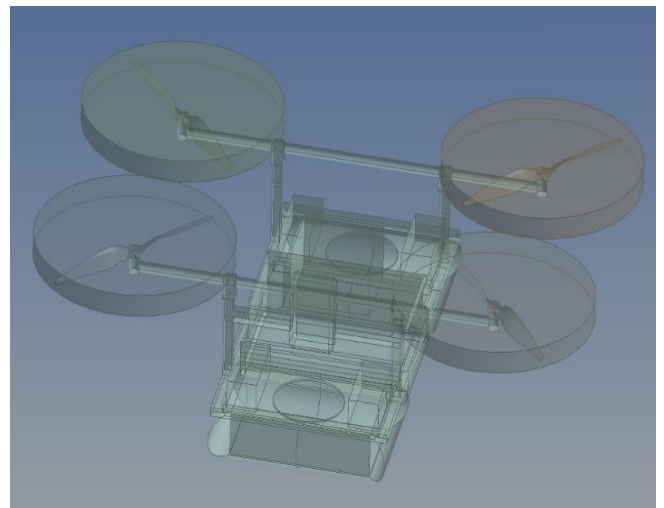


Fig. 2. UAV with MRF domain

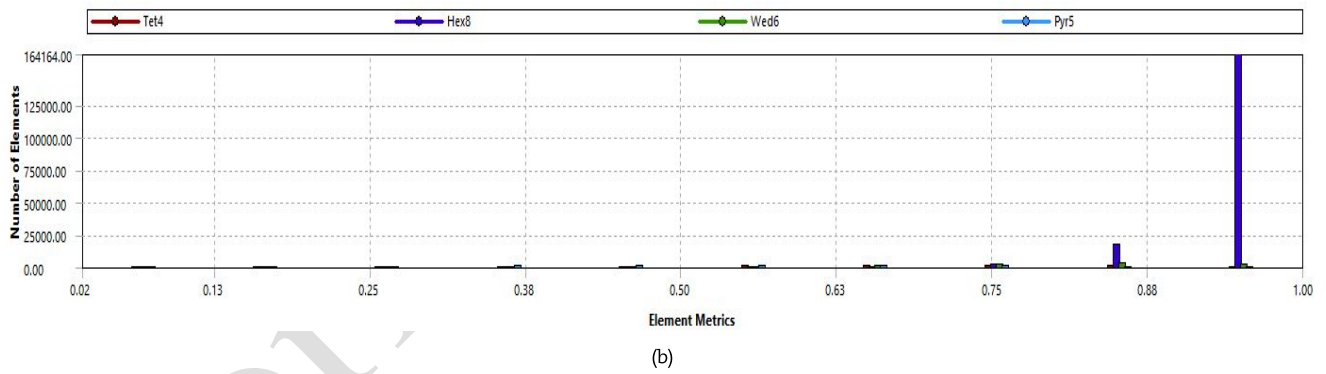
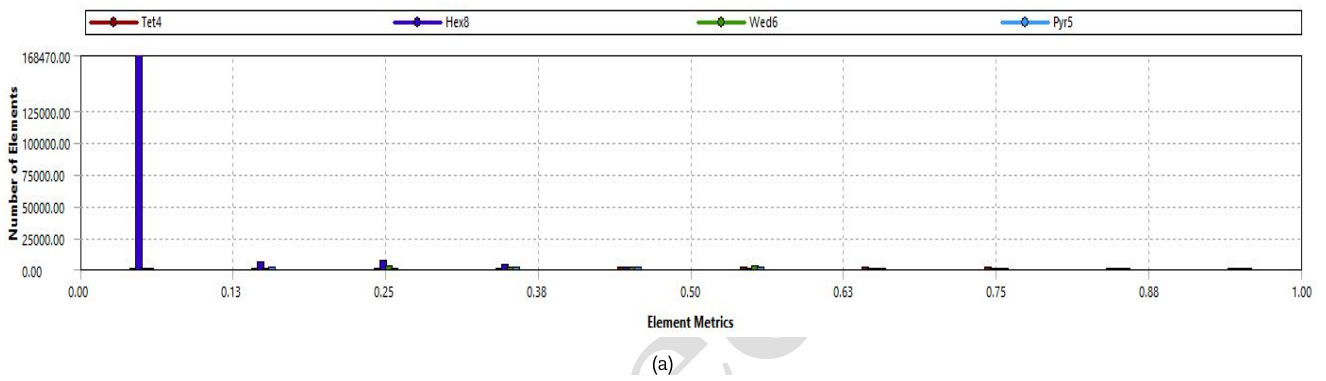


Fig. 3. Skewness and Orthogonal check: (a) Skewness (b) Orthogonality.

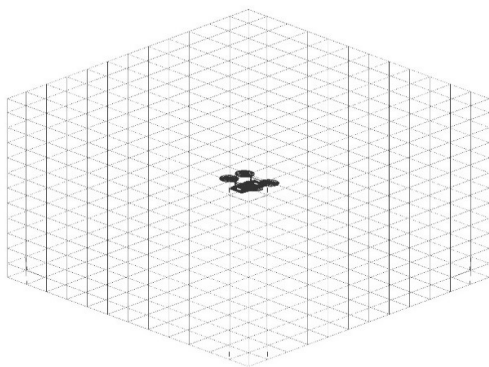


Fig. 4. Fluid – Structure domain

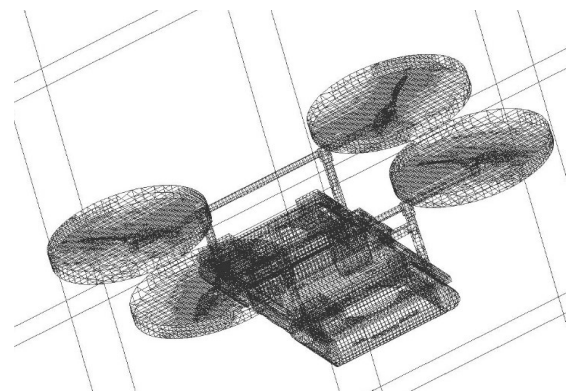


Fig. 5. Structured meshing of UAV

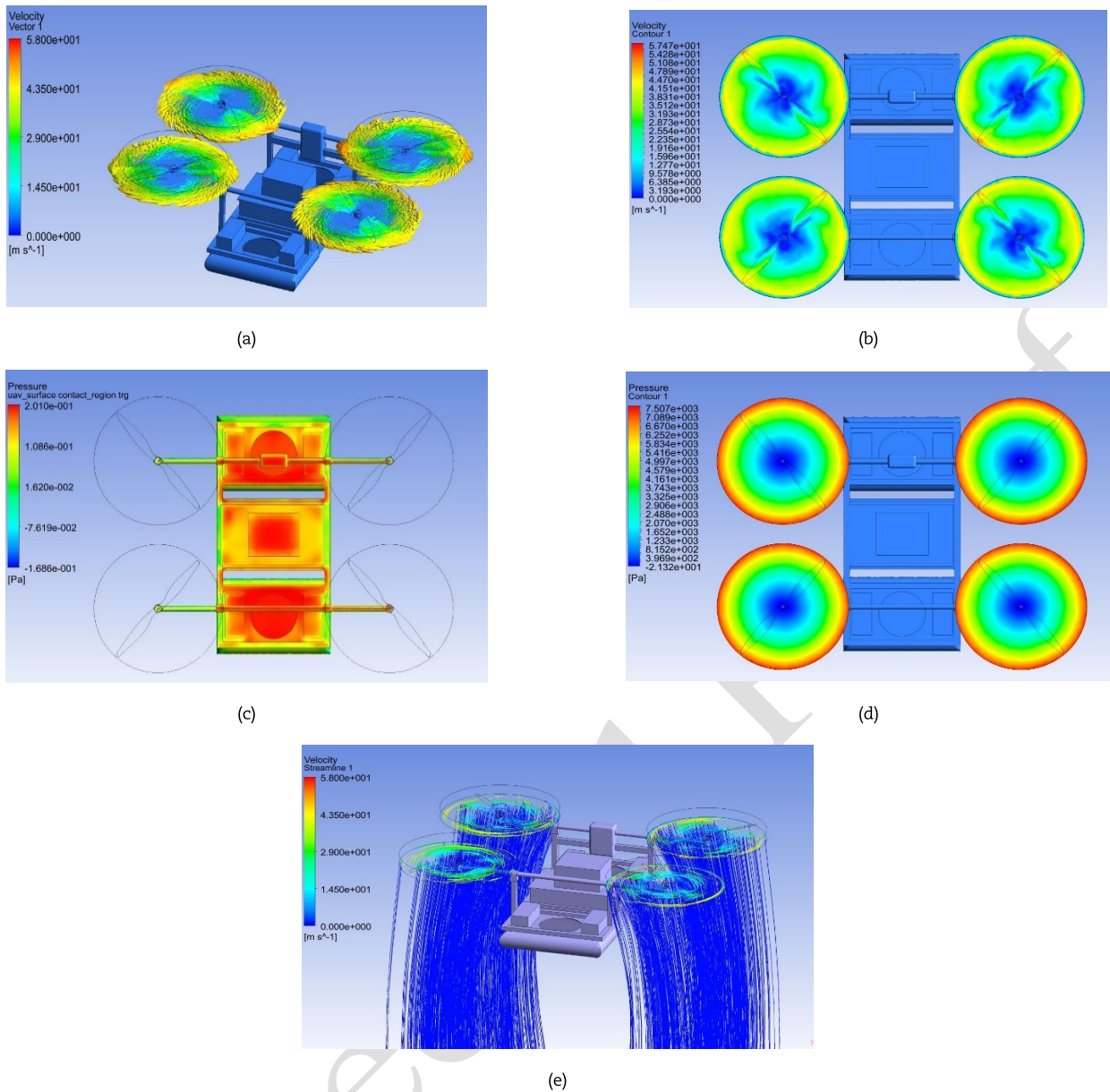


Fig. 6. Hovering condition results: (a) Vector plot; (b) Velocity contour; (c) Pressure contour on UAV; (d) Pressure contour on the Propeller Fan; (e) Velocity streamline.

4. Flow Analysis without Canopy

4.1 Hovering Phase

In order to simulate the hovering condition of UAV, all four rotors are given as constant speed of 5000 rpm using MRF model. CFD analysis is performed for the relative wind velocity of 0.5 m/sec, turbulent viscosity ratio of 10 and atmospheric pressure conditions. It is observed from the results of simulation, air flow interference between rotors and fuselage is considered to be minimal and it will not destabilize the UAV. Velocity vector plots depicted in Fig. 6(a) reveals uniform tip velocity of propellers is attained and velocity contour shown in Fig. 6(b) describes uniform distribution of velocity stagnation at the center of propeller and increases towards the tip and further decreases without any disturbances in flow conditions. The pressure distribution across the body of UAV is maximum as shown in Fig. 6(c) and at the tip of propeller has obtained maximum pressure (Fig. 6(d)). The uniform downstream velocity streamline confirms the hovering characteristics of UAV as observed in Fig. 6(e).

4.2 Forward Flight/pitching condition

The forward flight characteristics of UAV is analyzed for the relative velocity of 8.3 m/sec at 5°AoA (pitch down) in the atmospheric pressure conditions. The center of propeller is stagnant in nature and negligible velocity is experienced. However, velocity is increased further away from the center and reduced at the tip as shown in Fig. 7(a). Streamline of velocity in the forward direction of UAV shows that the air flow is not disturbed as shown in Fig. 7(b). Pressure exerted on the UAV structure is maximum along the body of UAV (Fig. 7(c)) due to stagnation flow. In the forward condition of UAV, the rear two propellers experiencing maximum pressure which is observed in Fig. 7(d) (pitch down of propeller) due to the action of wind load in comparison to front propellers. Due to this pressure difference, turbulence kinetic energy is maximum at the advancing side of rear propellers as depicted in Fig. 7(e).

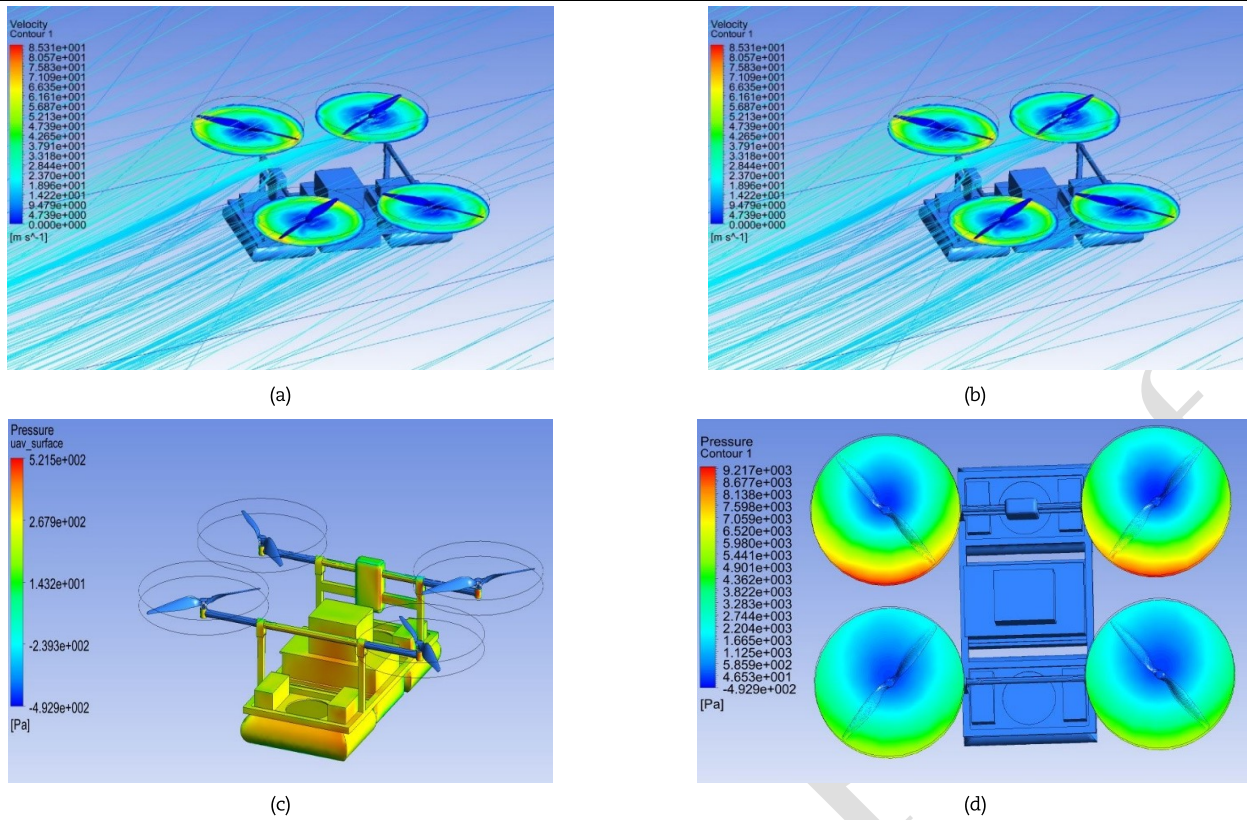


Fig. 7. Pitching condition: (a) Velocity contour; (b) Velocity streamline; (c) Pressure contour on UAV; (d) Pressure contour on propeller;

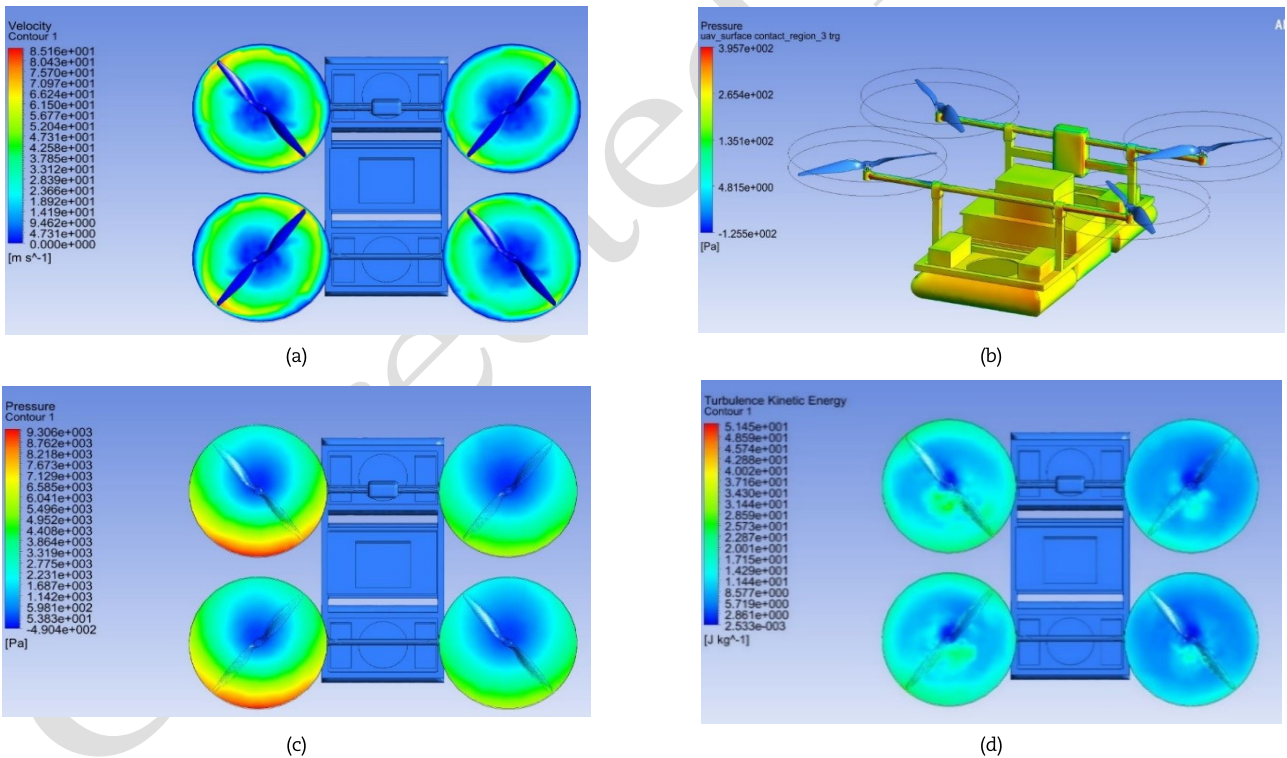


Fig. 8. Rolling condition: (a) Velocity contour; (b) Pressure contour on UAV; (c) Pressure contour on propeller; (d) Turbulence kinetic energy.

4.3 Rolling Condition

To attain rolling of the UAV, propellers 1 and 4 (left) is maintained at a speed of 5000 rpm and propellers 2 and 3 (right) rotated at 4000 rpm. It is evident from Fig. 8(a) that, there is an increase in tip velocity of propellers at the left side of UAV in comparison to the propellers right side of UAV due to rolling behaviour. The distribution of pressure is maximum at the right side of UAV because of the fact that, flow interference of 2 and 3 rotors exerting pressure of about 300Pa (Fig. 8(c)). However it is minimal that would not destabilize the UAV. The left side of the propeller experiencing the higher pressure in the advancing side compared to the right side of the propeller. It is due to the rolling manoeuvre condition. This pressure variation induces the high energized flow and it will eventually increase the turbulence kinetic energy rate in the left side rotors of the UAV which is clearly visible in the Fig. 8(d). This variation of turbulence kinetic energy in each rotors are minimal level that ensures the aerodynamic stability in rolling manoeuvre.



4.4 Yawing Condition

The propellers 2 and 4 are maintained at a speed of 5000 rpm and propellers 1 and 3 are rotated at 4000 rpm to achieve yaw motion. High tip velocity is experienced at 2 and 4 propellers because of high speed rotation as shown in Fig. 9(a) and there seems to be high cross flow interaction between these two propellers are obtained. The leading edge of propellers 2 and 4 are having higher pressure gradient as depicted in Fig. 9(b). The pressure distribution across the UAV (Fig. 9(c)) is uniform which guarantees the stability of the vehicle. The turbulence kinetic energy (Fig. 9(d)) at the propellers 2 and 4 are higher due to high tip velocity and increases from chord to tip. The flow interaction of the UAV under yawing condition is seen from the Fig. 9(e) dictates that the flow is influenced through the main body and velocity streamlines are uniform where in higher flow velocity occurs at propellers 2 and 4. The blade –vortex interaction event is induced at the rotors resulting in tip vortex as observed in Fig. 9(e).

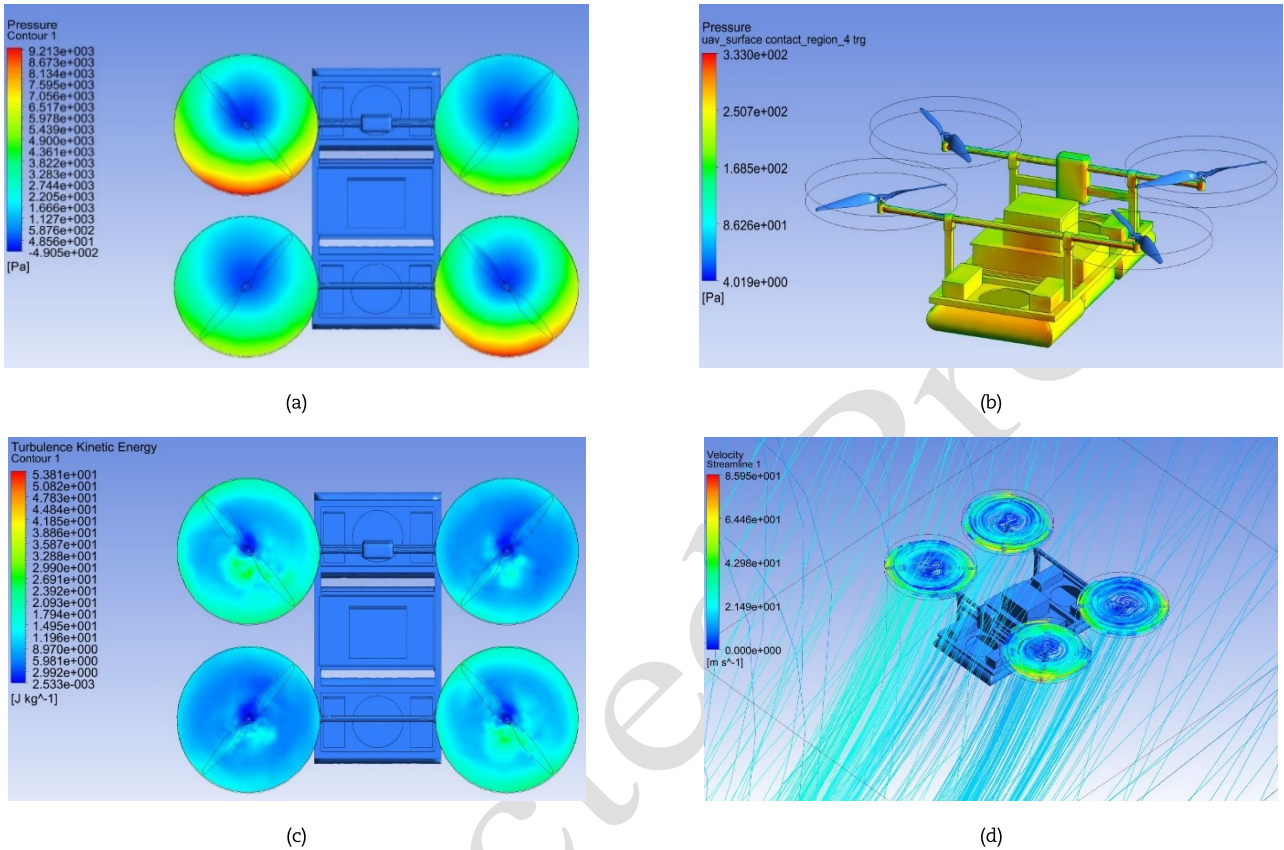
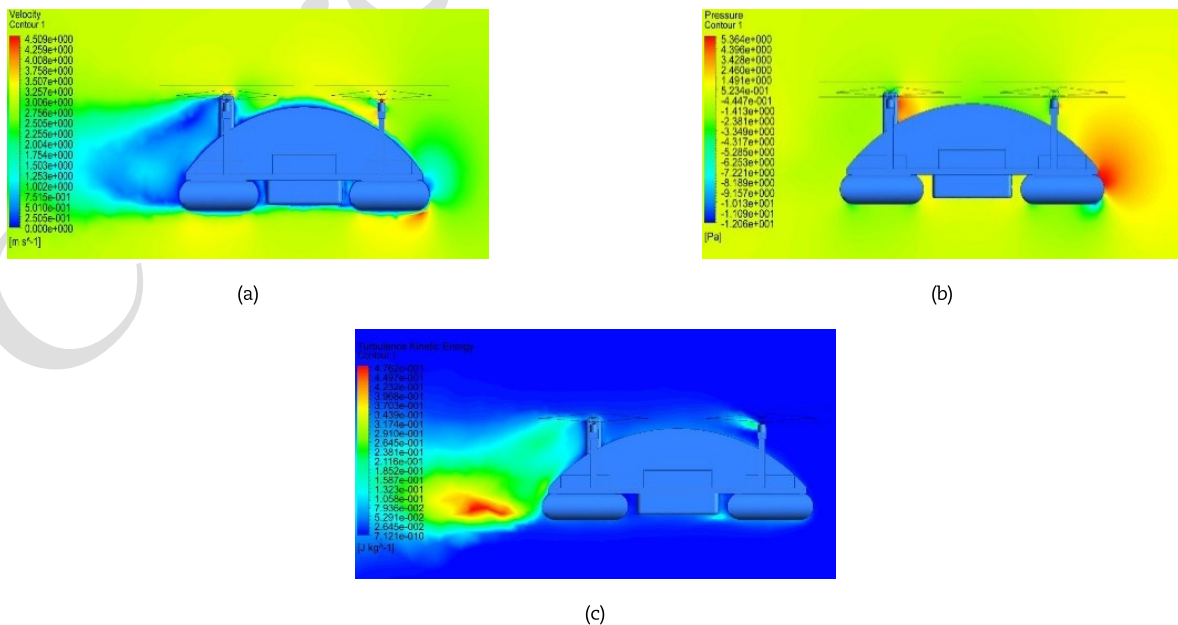
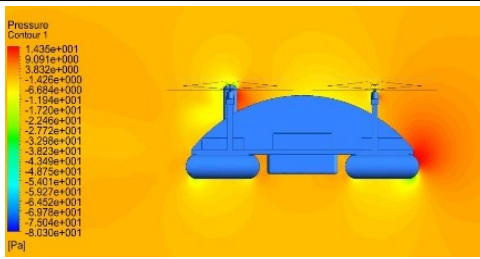


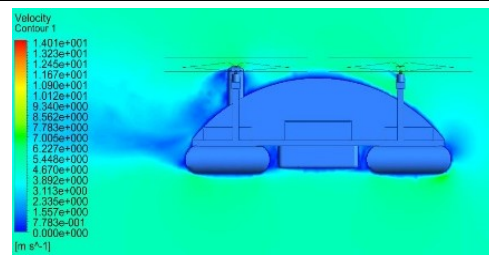
Fig. 9. Yawing condition: (a) Pressure contour on propeller; (b) Pressure contour on UAV; (c) Turbulence kinetic energy; (d) Velocity streamline.



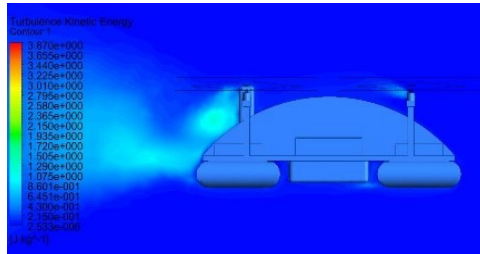
A: Free stream of velocity $V_{\infty}=3\text{ m/s}$



(d)

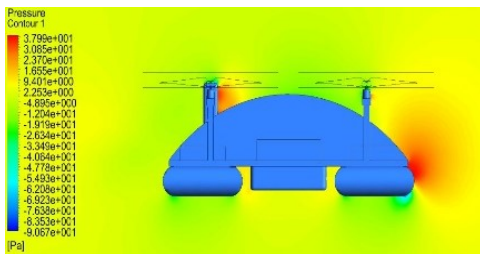


(e)

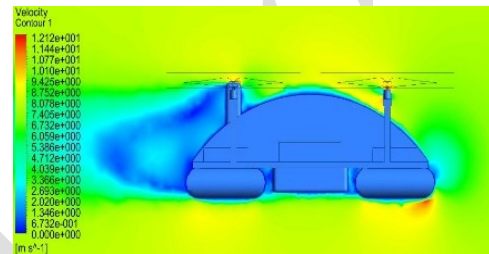


(f)

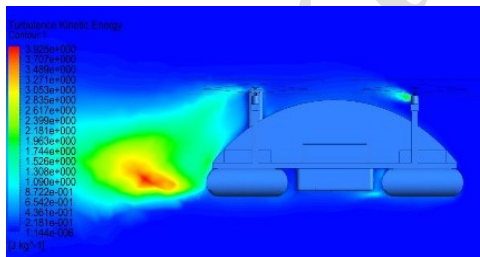
B: Free stream of velocity $V_{\infty}=5$ m/s



(g)

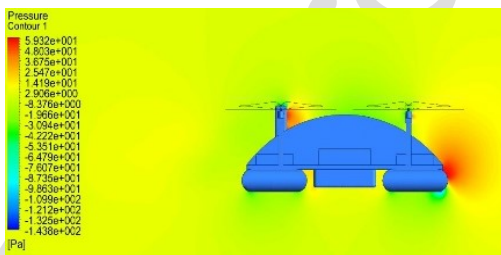


(h)

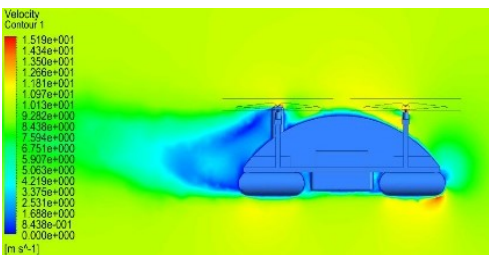


(i)

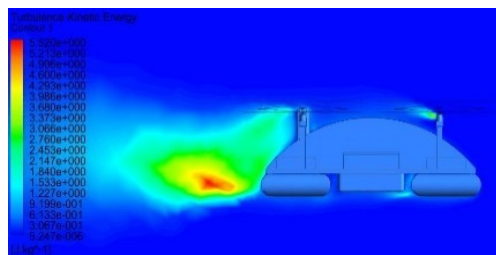
C: Free stream of velocity $V_{\infty}=8$ m/s



(j)



(k)



(l)

D: Free stream of velocity $V_{\infty}=10$ m/s

Fig. 10. Pressure, Velocity and Turbulence kinetic energy contour. A: Free stream of velocity $V_{\infty}=3$ m/s: (a) velocity; (b) pressure; (c) turbulent energy; B: Free stream of velocity $V_{\infty}=5$ m/s: (d) velocity; (e) pressure; (f) turbulent energy; C: Free stream of velocity $V_{\infty}=8$ m/s: (g) velocity; (h) pressure; (i) turbulent energy; D: Free stream of velocity $V_{\infty}=10$ m/s: (j) velocity; (k) pressure; (l) turbulent energy;

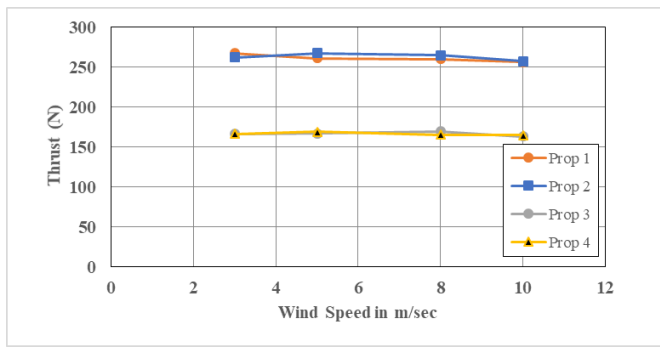


Fig. 11. Forward flight condition at 5° AOA

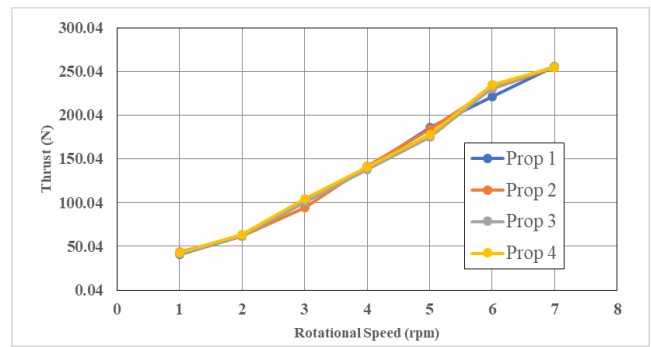


Fig. 12. Estimation of thrust

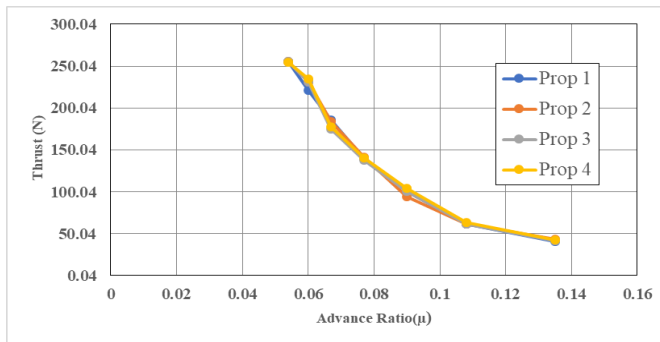


Fig. 13. Influence of thrust on Advance ratio

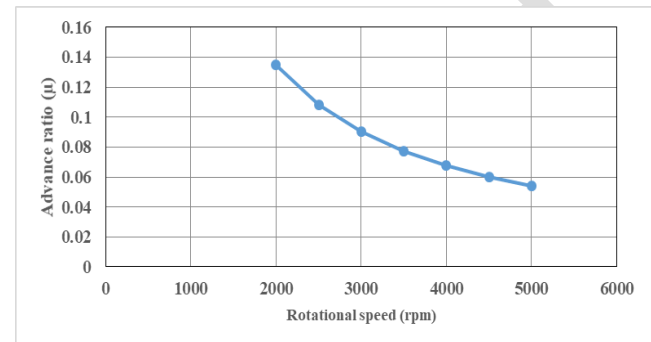


Fig. 14. Influence of rotor speed in Advance ratio

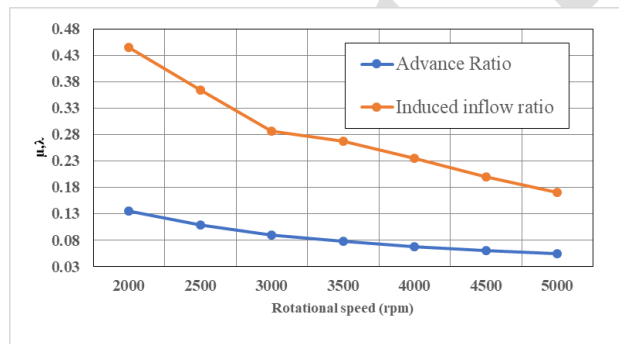


Fig. 15. Prediction of induced flow ratio

5. CFD Analysis with Canopy

5.1 Forward Condition

CFD analysis is carried out with introducing a canopy at the middle of the main body structure to reduce drag force on the surface of UAV. The speed is maintained in a way such that forward flight condition is obtained i.e., propellers 1 and 2 are operated at a speed of 5000 rpm and propellers 3 and 4 are operated at a speed of 4000 rpm. UAV is tested under different free stream velocities of 3, 5, 8 and 10 m/s. Under the free stream velocity of 3 m/s uniform distribution of pressure (Fig. 10_A) across the UAV is obtained. A high stagnation pressure at the front end of the UAV and propeller 3 and 4 are experienced. The flow velocity decreases at the rear end due to the adverse pressure gradient experienced and the kinetic energy associated with eddies seems to increase at the rear end owing to high eddy formation. The pressure distribution is highly uniform in case of free stream velocity of 5 m/s (Fig. 10_B) with least eddy formation and adverse pressure gradient. The flow characteristics at free stream velocity of 8 m/s (Fig. 10_C) are similar to that of 3m/s other than the flow at the rear end of UAV in which the flow is turbulent rather than in transient state for the free stream velocity of 3m/s. At free stream velocity of 10 m/s (Fig. 10_D) the boundary layer is fully developed at the rear end of the UAV with considerable eddies and reverse flow i.e. the flow is dominated with the separation and strong interaction. Also, interactions in wakes appear to be less strong with canopy as it blocks the interaction.

5.1.1 Effect of varying wind speed

For various wind speeds 3,5,8 and 10 m/sec and at an angle of attack 5° simulations are performed to examine the thrust characteristics of amphibious UAV. Since the flight path condition is to be maintained at forward conditions, the propellers 1 and 2 are retained at 5000 rpm as compared to the propellers 3 and 4 which are rotating at a speed of 4000 rpm. The thrust force produced by the propellers are tabulated (Table I.) and is seen that the effect of wind speed variation on the thrust is not very significant. There can be large regions of flow separation, with significant aerodynamic interaction between the non-rotating and rotating components of the system due the bluff aft regions. It is evident from Fig. 11 that the thrust produced by pair of propellers (1 and 2) and (3 and 4) are equal in magnitude and later is higher due to high speed of rotation.

Table 1. Thrust produced by each propeller at different Wind speed

| Wind speed(m/s) | 3 | 5 | 8 | 10 | |
|-----------------|--------|--------|--------|--------|--------|
| Thrust (N) | Prop 1 | 267.68 | 266.32 | 260.09 | 256.41 |
| | Prop 2 | 266.15 | 267.96 | 261.2 | 257.47 |
| | Prop 3 | 166.66 | 167.06 | 169.64 | 163.23 |
| | Prop 4 | 166.61 | 169.19 | 165.53 | 165.08 |

5.2 Hovering Phase

In hovering phase, the UAV is tested for the thrust produced by all the propellers rotating at diverse speeds ranging from 2000 to 5000 rpm with a relative wind velocity of 8.3m/s. It is seen from Fig. 12 that, thrust produced by the propellers is increasing linearly when the speed increases.

The effect of advance ratio is also studied and it is defined as the ratio of the free stream speed to the propeller speed, which is non dimensional significance for propeller's velocity. Generally, when the propeller runs at a higher speed, the advance ratio would be small and reverse is true. The relation between the advance ratio and the thrust produced by the corresponding propeller is shown in Fig.13 and signifies the thrust increases with increase in the advance ratio.

Advance ratio is calculated with reference to relative wind velocity of 8 m/sec and 5° AoA. Speed of propeller is inversely proportional to advance ratio and the same can be visualized from the Fig. 14. The comparisons of the advance ratio and the induced flow ratio i.e. the ratio of total inflow velocity to rotor tip speed against the rotational speed shows (Fig. 15) similar in trend. However, the advance ratio and the inflow ratio are inversely proportional to the propeller speed and hence they are decreasing.

6. Conclusion

In this article, aerodynamic interactions of novel amphibious vehicle in roll, pitch, yaw, forward and hovering flight conditions are analyzed using CFD platform. The flow around the UAV, velocity and pressure distribution across the rotors are attained uniformity in distribution and stability of the vehicle is ensured. The tip of the propellers obtained maximum pressure during hovering. However, in the forward condition of UAV, the rear two propellers experienced maximum pressure and due to which turbulence kinetic energy is maximum at the advancing side of rear propellers. In the event of rolling, left side of the propeller experiencing the high pressure in the advancing side compare to the right side of the propeller. However, in the case of yawing, the leading edge of propellers 2 and 4 are having higher pressure than other two propellers. The CFD studies on amphibious UAV with and without canopy resulted in minimal drag of about 15% reduction is achieved. Rotor interactions for diverse speed conditions ranging from 2000 to 5000 rpm under hovering and forward conditions provided greater insight on flow characteristics around the UAV, advancing and retreading side obtained uniform distribution of pressure The thrust force generated from the pair of propellers are equal in magnitude and maximum thrust of 267 N is experienced in the propellers. The pair of propellers such as (1 and 2) and (3 and 4) have generated equal amount of thrust (0.5% deviation) and hence the smooth flight is guaranteed. The effect of increase in speed of propeller on non-dimensional relationship such as advance ratio and induced-inflow ratio signifies they are inversely proportional to speed. The CFD analysis results predicted that, at 5° AoA and 8 m/sec, the aerodynamic performance is superior and it is considered to be the best operating condition for the amphibious UAV in performing various missions including water quality monitoring in remote water bodies.

Author Contributions

B. Esakki is the principal investigator for this project. He has contributed in writing the entire manuscript; L.J. Yang is the partner for this project. He has provided scientific and technical interpretation of CFD analysis results and also contributed in technical writing of the manuscript; G. Raj has performed CFD analysis of without canopy model; E. Khurana and S. Khute contributed in the CFD analysis with canopy model; P. Vikram has contributed in the modeling, meshing and preliminary investigations for CFD analysis.

Conflict of Interest

The authors declared no potential conflicts of interest with respect to the research, authorship and publication of this article.

Funding

Authors would like to thank the funding supported by DST – GITA (Ref: 2015RK0201103) under Indo-Korea collaborative research programme.

References


- [1] Hildmann, H. Kovacs, E. Saffre, F. Isakovic, F., Nature-inspired drone swarming for real-time aerial data-collection under dynamic operational constraints, *Drones*, 3(3), 2019, 71.
- [2] Esakki, B., Ganesan, S., Mathiyazhagan, S., Design of amphibious vehicle for unmanned mission in water quality monitoring using IoT, *Sensors*, 18(10), 2018, 3318.
- [3] Diaz, P., and Yoon, S., High-fidelity computational aerodynamics of multi-rotor unmanned aerial vehicles, *AIAA SciTech Forum*, Kissimmee, FL, USA, 2018.
- [4] Diaz, P., Yoon, S., and Theodore, C. R., High-fidelity computational aerodynamics of the Elytron 4S UAV, *AHS Specialists Meeting - Aeromechanics*, San Francisco, CA, USA, 2018.
- [5] Thibault, S., Holman, D., Trapani, G., Garcia, S., CFD Simulation of a Quad-Rotor UAV with Rotors in Motion Explicitly Modeled Using an LBM Approach with Adaptive Refinement, *55th AIAA Aerospace Sciences Meeting*, 9-13 January, Grapevine, Texas, USA, 2017.
- [6] Setijl, R., Baracos, G.N., Computational study of helicopter rotor-fuselage aerodynamic interaction, *AIAA Forum*, 47(9), 2009, 2143.
- [7] Antoniadis, A.F., Drikakis, D., Zhong, B., Baracos, G., Steijl, R., Biava, M., Embacher, M., Assessment of CFD methods against experimental flow measurements for helicopter flows, *Aerospace Science and Technology*, 19(1), 2012, 86-100.
- [8] Boon, M.A., Drijfhout, A.P., Tesfamichael, S., Comparison of a fixed-wing and multi-rotor uav for environmental mapping applications: a case study, *International Conference on Unmanned Aerial Vehicles in Geomatics*, 4-7 September, Bonn, Germany, 2017.
- [9] Viieru, D., Tang, J., Lian, Y., Liu, H., Shyy, W., Flapping and Flexible Wing Aerodynamics of Low Reynolds Number Flight Vehicles, *44th AIAA Aerospace Sciences Meeting and Exhibit*, Reno, Nevada, USA, 2006.


- [10] Biava, M., Khier, W., Vigevano, L., CFD prediction of air flow past a full helicopter configuration, *Aerospace Science and Technology*, 19(1), 2012, 3-18.
- [11] Tytus T., Low Reynolds Number Rotor Blade Aerodynamic Analysis, MATEC Web Conf., 252, 2019, 04006.
- [12] Pérez Gordillo, A.M., Villegas Santos, J.S., Lopez Mejia, O.D., Suárez Collazos, L.J., Escobar, J.A., Numerical and Experimental Estimation of the Efficiency of a Quadcopter Rotor Operating at Hover, *Energies*, 12, 2019, 261.
- [13] Celic, A., Hirschel, E.H., Comparison of eddy-viscosity turbulence models in flows with adverse pressure gradient, *AIAA Journal*, 44(10), 2006, 2156-2169.
- [14] Boyd, Jr.D., Barnwell, R., Gorton, S., A computational model for rotor-fuselage interactional aerodynamics, *The 38th Aerospace Sciences Meeting and Exhibit*, NASA Langley Technical Report Server, 2000, p. 256.
- [15] He, C., Nischint, R., Modeling the Aerodynamic Interaction of Multiple Rotor Vehicles and Compound Rotorcraft with Viscous Vortex Particle Method, *American Helicopter Society 72nd Annual Forum At: West Palm Beach*, FL, USA, 2016.
- [16] Ye, L., Zhang, Y., Yang, S., Zhu, X., Dong, J., Numerical simulation of aerodynamic interaction for a tilt rotor aircraft in helicopter mode, *Chinese Journal of Aeronautics*, 29(4), 2016, 843-854.
- [17] CaO, Y.H., Yu, Z.Q., Yuan, S.U., Kai, K., Combined free wake/CFD methodology for predicting transonic rotor flow in hover, *Chinese Journal of Aeronautics*, 15(2), 2002, 65-71.
- [18] Conlisk, A.T., Modern helicopter rotor aerodynamics, *Progress in Aerospace Sciences*, 37(5), 2001, 419-476.
- [19] Dindar, M., Shephard, M.S., Flaherty, J.E., Jansen, K., Adaptive CFD analysis for rotorcraft aerodynamics, *Computer Methods in Applied Mechanics and Engineering*, 189(4), 2000, 1055-1076.
- [20] Dometge, P.X.C., Ilie, M., Numerical study of helicopter blade-vortex mechanism of interaction using the potential flow theory, *Applied Mathematical Modelling*, 36(7), 2012, 2841-2857.
- [21] Felismina, R., Silva, M., Mateus, A., Malça, C., Study on the aerodynamic behavior of a UAV with an applied seeder for agricultural practices, *AIP Conference Proceedings*, 1836(1), 2017, 020049.
- [22] Filippone, A., Michelsen, J.A., Aerodynamic drag prediction of helicopter fuselage, *Journal of Aircraft*, 38(2), 2001, 326-333.
- [23] Qijun, Z., Zhao, G., Wang, B., Wang, Q., Shi, Y., Xu, G., Robust Navier-Stokes method for predicting unsteady flow field and aerodynamic characteristics of helicopter rotor, *Chinese Journal of Aeronautics*, 31(2), 2014, 214-224.
- [24] Shi, Y., Xu, Y., Xu, G., Wei, P., A coupling VWM/CFD/CSD method for rotor air load prediction, *Chinese Journal of Aeronautics*, 30(1), 2017, 204-215.
- [25] Tan, J., Wang, H., Panel/full-span free-wake coupled method for unsteady aerodynamics of helicopter rotor blade, *Chinese Journal of Aeronautics*, 26(3), 2013, 535-543.
- [26] Lopez, O.D., Escobar, J.A., Pérez, A.M., Computational Study of the Wake of a Quadcopter Propeller in Hover, *The 23rd AIAA Computational Fluid Dynamics Conference*, 2017, p. 3961.
- [27] Thibault, S., Holman, D., Garcia, S., Trapani, G., CFD Simulation of a quad-rotor UAV with rotors in motion explicitly modeled using an LBM approach with adaptive refinement, *The 55th AIAA Aerospace Sciences Meeting*, 2017, p. 583.
- [28] Yoon, S., Lee, H.C., Pulliam, T.H., Computational analysis of multi-rotor flows, *The 54th AIAA Aerospace Sciences Meeting*, 2016, p. 812.


ORCID iD


Balasubramanian Esakki  <https://orcid.org/0000-0003-4663-4132>

P. Gokul Raj  <https://orcid.org/0000-0003-2380-9286>

Lung-Jieh Yang  <https://orcid.org/0000-0002-0639-0973>

P. Vikram  <https://orcid.org/0000-0002-0328-194x>

Ekanshu Khurana  <https://orcid.org/0000-0003-1486-3416>

Sahadasan Khute  <https://orcid.org/0000-0002-5080-4328>



© 2020 by the authors. Licensee SCU, Ahvaz, Iran. This article is an open access article distributed under the terms and conditions of the Creative Commons Attribution-NonCommercial 4.0 International (CC BY-NC 4.0 license) (<http://creativecommons.org/licenses/by-nc/4.0/>).

How to cite this article: Esakki B., Gokul Raj P., Yang L.J., Vikram P., Khurana E., Khute S. Computational Fluid Dynamic Analysis of Amphibious Unmanned Aerial Vehicle, *J. Appl. Comput. Mech.*, 7(1), 2021, x-xx. <https://doi.org/10.22055/JACM.2020.32461.2018>